DESIGN, SYNTHESIS, ANTI-CANCER ACTIVITY, AND MOLECULAR DOCKING STUDIES OF LIGNAN-PYRROLE DERIVATIVES AS A JAK3 INHIBITOR

NISHA CHIRIAPANDA LOHITH[1], RANJINI PUTTASWAMY[2], DEVARAJU[1]*

[1]Department of Chemistry, Yuvaraja's College, University of Mysuru, Mysuru, Karnataka, India. [2]Department of Biotechnology, SIR M V Government Science College, Badravati, Shivamogga, Karnataka, India.
*Corresponding author: Devaraju; Email: devarajuycm.01@gmail.com

ABSTRACT

Objectives: The aim of the study was to predict the interaction patterns between poly (ADP-ribose) polymerase (PARP), vascular endothelial growth factor receptor (VEGFR1), and Janus kinase 3 (JAK3) with LIGNAN-pyrrole derivatives using molecular docking studies. *In vitro* anti-cancer activity of LIGNAN-pyrrole derivatives on HeLa cells.

Methods: The key proteins such as PARP, Rad18, VEGFR1, JAK3, alpha-beta tubulin, SarA, Rad6, VEGFR2, leukocyte type core 2 beta 1, 6-N-acetylglucosaminyltransferase,and epidermal growth factor receptor kinase domain were retrieved from the protein data bank. The effect of compounds on cell proliferation of HeLa cells was determined by MTT assay. The cell was treated with or without compound and was incubated for 48 h.

Results: The cytotoxicity assay was performed for the initial screening of LIGNAN-pyrrole derivatives. Among the tested molecules, compound **4b** emerged to be potent against HeLa cells at lower concentrations.

Conclusion: Molecular docking studies revealed that the screened compounds are found to be good PARP, VEGFR1, and JAK3 inhibitors. *In vitro* screening proved that the compounds can be good antiproliferative agents.

Keywords: Regioselective, Pyrrole, Anti-cancer, HeLa, Molecular docking.

INTRODUCTION

One of the serious problems that the global health system facing today is to combat cancer in effective manner [1,2]. Cancer is a disease with uncontrolled growth and spread of cells, these proliferating cells rapidly divide and miscommunicate among cells and end up with DNA damage [3-5]. Blood, breast, lung, prostate, and colon cancers are most common among different types of cancer [6]. All of these cancers are considered the most aggressive and life-threateing malignancies. Although they are sensitive to chemotherapeutic agents, there are only limited effective chemical entities that are presently used [7,8]. Janus kinase 3 (JAK3) signaling pathway plays a key role in the pathogenesis of human cancer [9]. Vascular endothelial growth factor receptor (VEGFR) is typical tyrosine kinase receptors closely linked to angiogenesis regulatory systems and they are important target for anti-angiogenic therapy in cancer [10]. Poly(ADP-ribose) polymerase (PARP) is a protein involved in DNA repair of single strand breaks, makeing them an interesting target for cancer therapy. PARP inhibitors specifically target cancer cells in BRCA-mutation cancer cells over normal cells [11]. In general, targeting JAK3 signaling, VEGFR and PARP through small molecule inhibitors could be an ideal approach to fight against cancer.

Small molecule inhibitors have become the prime source for the invention of new drug molecules [12-17]. Specific molecules with pyrrole ring play an important role in medicinal and bio-organic chemistry as theirnuclei are present in many natural products [18,19]. They serve as precursors to construct lot of pharmaceutical agents and interestingly many drugs, especially anti-cancer drugs such as sunitinib, neolamellari, ulixertinib, prodigiosin, semaxanib, orantinib, vorolanib, and toceranib (Fig. 1) contain pyrrole core [20]. Many efforts have been made to construct pyrrole-based bioactive compounds includingcycloaddition, simple cyclization, and cyclocondensation reactions catalyzed by various catalysts from different synthetic building blocks [21]. Despite of being very good bioactive nucleus, there are very few methods have been reported to construct highly substituted pyrrole derivatives. Recently, we have reported a highly efficient transition metal-free regioselective synthesis of 2,3,5-trisubstituted-pyrroles from the corresponding β-enaminone building blocks [22].

In continuing synthetic efforts [23-32] to further explore the synthetic potential of carbonyl compound precursors, we herein report the selective reactivity of 1,4-dicarbonyl compound toward nucleophilic amines. In continuation of identifying new biologically active scaffolds [33-40], we have screened the synthesized LIGNAN-pyrrole derivatives for their cytotoxicity effect against human cervical cancer HeLa cell lines and evaluated their antiproliferative property against HeLa cells using MTT assay. The IC_{50} values suggested that the compounds are sensitive to tested cell lines. To understand the mechanism of action in further, we have docked these compounds against various key proteins such as PARP, Rad18, VEGFR1, and JAK3. Results indicated that the synthesized compounds have potential to become PARP, VEGFR1, and JAK3 inhibitors.

METHODS

General

The reactions were observed through thin-layer chromatography (TLC) using silica gel G/UV-254 precoated sheets. Measured melting points were reported without any corrections. The ^{1}H and ^{13}C nuclear magnetic resonance (NMR) were obtained in BRUKER amx Fourier transform NMR spectrometer with operating frequencies of 400 and 100 MHz. Separation was performed using column chromatography with 60–120 mesh silica gel. Required 1,4-dicarbaldehyde **1** was prepared according to the reported methods.
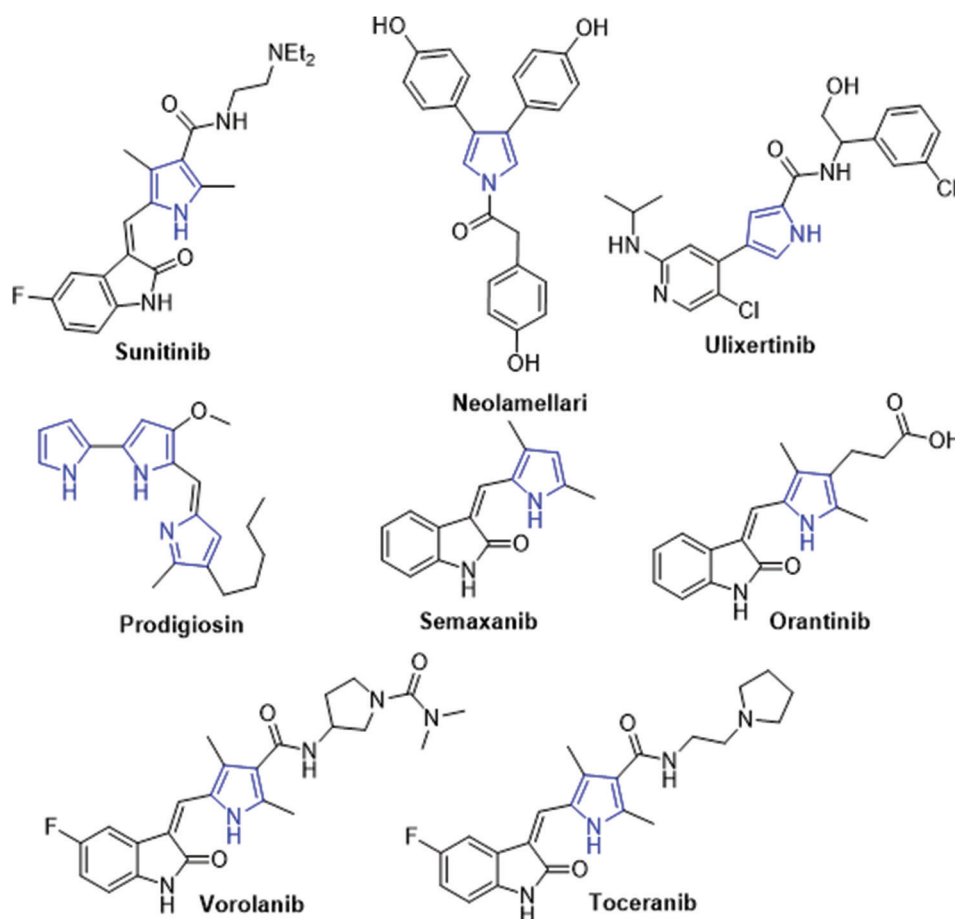
Fig. 1: Pyrrole containing anticancer drug molecules

General procedure for the preparation of compounds 3a-c

Compound **1 (**5 mmoL) and aniline **2a** or methyl amine **2b** (5 mmoL) or paratrifluoromethyl aniline (5 mmoL) were dissolved in toluene (25 mL) in round-bottom flask and refluxed for 6 h (monitored by TLC). The solvent was evaporated under reduced pressure and the residue was diluted with dichloromethane and water. The organic layer was washed with brine and evaporated to give crude products which were purified by column chromatography.

General procedure for the preparation of title compounds 4a-c

Compounds **3a-c** (1.0 mmoL) and Pd/C (10 wt% of 10% Pd/C) were taken in methanol (15 mL). The reaction mixture was kept for 8 h at room temperature in a hydrogen atmosphere and the reaction was monitored by TLC. The reaction mixture was filtered and the solvent was removed and diluted with dichloromethane and water. The separated organic layer was concentrated to give crude products **4a-c** which were purified by column chromatography.

Characterisation data of compounds

4,4'-((1-phenyl-1H-pyrrole-3,4-diyl)bis(methylene))bis(2,6-dimethoxyphenol) (4a)

Off white solid; ^{1}H NMR (400 MHz, CDCl$_3$) δ 2.95–2.89 (m, 4H), 3.72 (s, 12H), 6.676 (s, 4H), 7.63-7.59 (m, 3H), 7.76-7.71 (m, 2H), 8.82 (s, 2H),; ^{13}C NMR (100 MHz, CDCl$_3$) δ 48.17, 56.21, 126.0, 127.3, 127.6, 127.7, 127.9, 129.0, 129.07, 129.3, 132.6.

4,4'-((1-methyl-1H-pyrrole-3,4-diyl)bis(methylene))bis(2,6-dimethoxyphenol) (4b)

Brown solid; ^{1}H NMR (400 MHz, CDCl$_3$) δ 2.32 (s, 3H), 2.94–2.88 (m, 4H), 3.71 (s, 12H), 6.68 (s, 4H), 8.79 (s, 2H); ^{13}C NMR (100 MHz, CDCl$_3$) δ 23.1, 48.17, 56.21, 122.6, 126.3, 129.0, 131.0, 132.1.

4,4'-((1-(4-(trifluoromethyl)phenyl)-1H-pyrrole-3,4-diyl)bis(methylene))bis(2,6 dimethoxyphenol) (4c)

Pure white solid; ^{1}H NMR (400 MHz, CDCl$_3$) δ 2.91–2.85 (m, 4H), 3.82 (s, 12H), 6.67 (s, 4H), 7.23–7.21 (d, *J* = 7.2 Hz, 2H), 7.54–7.53 (d, *J* = 7.2 Hz, 2H), 8.59 (s, 2H); ^{13}C NMR (100 MHz, CDCl$_3$) δ 47.1, 55.1, 125.5, 125.6, 125.7, 128.4, 128.5, 129.8, 130.8, 135.4, 135.5, 136.1, 136.6, 136.8.

MTT assay

The effect of compounds on cell proliferation of HeLa cells was determined by MTT assay. The cell was treated with or without compound and was incubated for 48 h. MTT reagent (5 mg/mL) was added and colored change due to proliferation cell was estimated.

Molecular docking

Molecular docking is one of the key methods in medicinal chemistry. The goal of ligand-protein docking is to forecast the dominant binding mode(s) of a ligand with a targeted protein having a known three-dimensional structure [41,42]. The key proteins such as PARP, Rad18, VEGFR1, JAK3, alpha-beta tubulin, SarA, Rad6, VEGFR2, leukocyte type core 2 beta1,6-N-acetylglucosaminyltransferase (C2GnT-L), and epidermal growth factor receptor (EGFR) kinase domain [43,44] were retrieved from the protein data bank. Water molecules from proteins were removed beyond 5 Å from the hetero atom, respectively, and catalytical water molecules were kept at the active site during protein preparation wizard and Optimized Potentials for Liquid Simulations-2005 (OPLS_2005) force field [45,46] was applied to the pre-processing of protein. After the protein was prepared, a grid generation was computed with a distance of 20 Å from the active site. The ligand structures 4a, 4b, and 4c were drawn using a 2D sketcher and energy minimize was computed by applying OPLS_2005. Using extra-precision docking

was docked into the receptor grid of radii 20 Å and the docking calculation was judged based on the docking score and hydrogen bond interactions.

Molecular mechanics-generalized born surface area (MM/GBSA)

The docked posture of the ligand was rescored using MM/GBSA. Because they are less computationally intensive than alchemical free energy methods and more accurate than most scoring functions of molecular docking, MM/GBSA is a routine method for predicting binding free energies. The energy of optimized free receptors, a free ligand, and a combination of the ligand and a receptor are all calculated by prime MM/GBSA [47].

Molecular dynamic simulations (MDSs)

MDS was operated out on a 64-bit Ubuntu 20.04 platform. MDSs for the compounds 4a, 4b, and 4c were carried out against JAK3, VEGFR1, and PARP which are the top scorer in molecular docking and MMGBSA were chosen for MDSs. For JAK3, the system was neutralized with the Na$^+$ ions (53.213 mM, with a charge of +31), and Cl$^-$ (51.497 mM, with a charge of −30) was added to the system. In the case of VEGFR1, the system was neutralized with the Na$^+$ ions (50.149 mM, with a charge of +27), and Cl$^-$ (63.151 mM, with a charge of −34) was added to the system. For PARP, the system was neutralized with the Na$^+$ ions (50.737 mM, with a charge of +34), and Cl$^-$ (52.229 mM, with a charge of −35) was added to the system. The simulation was carried out throughout 100 ns [48,49].

RESULTS

Synthesis of LIGNAN-pyrrole derivatives 4a-c

The synthetic potential of 1,4-dialdehyde precursor has been further explored for heterocyclic synthesis. Previously we have synthesized 2,3,5-tri substituted pyrrole derivatives majorly limited to an electron-withdrawing group (ester and cyano) substitution at the 2nd carbon atom in the pyrrole ring [22]. Formation of 2,3,5-tri substituted pyrroles with different aryl and/or heteroaryl groups on pyrrole ring were not satisfactory in the reported method. Since ester and cyano groups can easily undergo hydrolysis under physiological conditions, we are thinking of installing stable substituents even on the second position of pyrrole moiety in the form of aryl or heteroaryl groups, thereby increasing the bioavailability of the compounds. In the present study, we are constructing pyrrole ring in the LIGNAN structure with aryl/alkyl groups on nitrogen atom of pyrrole ring using different aryl/methyl amines. Condensation of aniline **2a**, methylamine **2b** and paratrifluoromethyl aniline **2c** with 1,4-dicarbaldehyde **1** underwent smoothly in toluene solvent under reflux condition to give corresponding intermediates **3a-c**, which upon debenzylation reaction in presence of Pd/C and hydrogen atmosphere at room temperature to produce the title compounds **4a-c** in good yields as shown in Scheme 1 and Table 1.
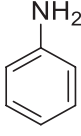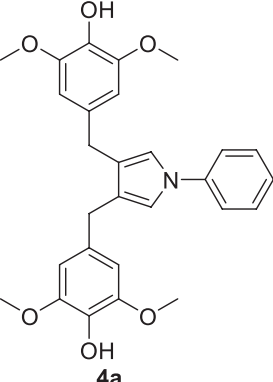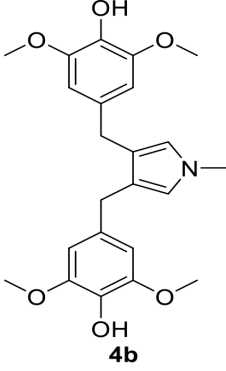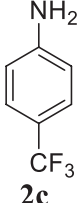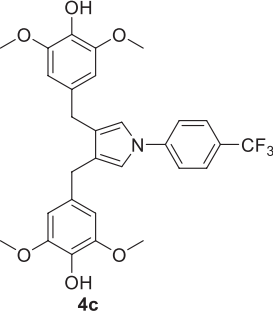
DISCUSSION

Compounds 4a, 4b, and 4c induces cytotoxicity on HeLa cell lines

Inhibition of cell proliferation is a key phenomenon for chemotherapeutic agents. In the current study, we have tested the anti-proliferative and cytotoxicity effect of compounds **4a**, **4b**, and **4c** against human cervical cancer HeLa cells. The obtained IC$_{50}$ values against HeLa cell lines were assessed by MTT assay (Fig. 2a and b). It is apparent from the results that HeLa cell lines were sensitive to compounds **4a**, **4b**, and **4c** which have repressed the proliferative efficiency in HeLa cell lines and showed a significant reduction in cell viability compared to positive control upon treatment with **4a-c**.
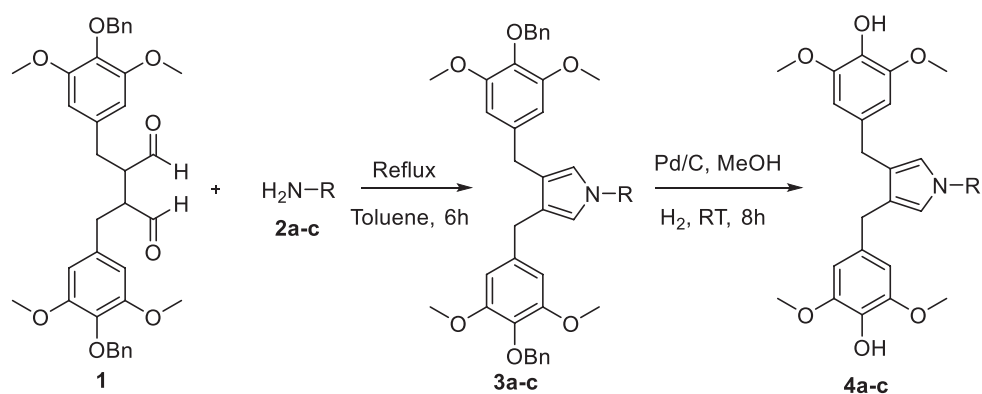
Molecular docking studies

Drug design techniques are becoming more and more interested in molecular docking, particularly in light of its notable potential for carrying out effective virtual screening campaigns [50]. A large chemical library may be simulated on a large panel of targets using the current computational resources in a reasonable amount of time, and these exceptionally long simulations seem to be particularly

Table 1: Synthesis of LIGNAN-pyrroles 4a-c from 1,4-dicarbonyl compound 1

Entry	2	4	Yield^a %
1	**2a**	**4a**	70
2	**2b**	**4b**	68
3	**2c**	**4c**	65

^{a}Isolated Yield

useful for multi-target ligand design as well as repurposing research. Therefore, key proteins which come across better anti-cancer activity were chosen for molecular docking to study its inhibition with the potent ligands followed by MM/GBSA and molecular dynamics studies to investigate the possible binding geometry of the ligand. The geometrical binding pose of the potent ligand was predicted by a molecular docking investigation for the ligand. A molecular docking study revealed that the ligand **4a, 4b**, and **4c** are very potent against key proteins listed in Tables 2a and b. Ligand **4a** occupied the ATP binding site of JAK3 with a promising docking score of −9.7 kcaL/moL (Table 2a), whereas ligand **4b** binds tightly to VEGFR1 with a docking score of −9.1 kcaL/moL. Ligand 4c interacts with PARP with a docking score of −8.15 kcaL/moL. These ligands with respective targeted proteins are the key mediators for progression of cancer with the promising molecular dock scores. When these ligands **4a, 4b**, and **4c** were further screened for the other key proteins such as alpha-beta tubulin, SarA, Rad6, VEGFR2, C2GnT-L, and EGFR kinase domain to check its efficiency, these ligands **4a, 4b**, and **4c** were poorly interacted (Table 2b). To validate the molecular docking scores, we performed MM/GBSA.

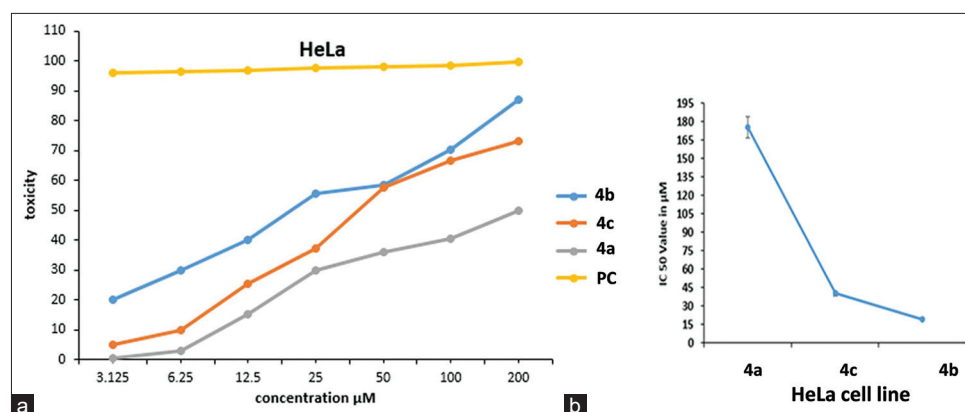**Scheme 1: Two-step synthesis of LIGNAN-pyrrole derivatives 4a-c**

Fig. 2: (a) Toxicity studies against HeLa cell lines. (b) IC$_{50}$ values assessed by MTT assay

Table 2a: Molecular docking and MMGBSA for the compounds 4a, 4b, and 4c against various key proteins such as PARP, Rad18, VEGFR1, and JAK3

PDB ID	Ligands	Molecular docking (kcaL/moL)			MMGBSA ΔG bind (kcaL/moL)					
		Docking score	Glide energy	HBond	Total	Coulomb	Hbond	Lipo	Packing	vdW
2RCW	4a	−7.71	−48.64	−2.21	−44.96	−3.87	−0.61	−25.41	−2.66	−42.02
	4b	−6.77	−41.78	−0.41	−50.18	−16.06	−1.14	−24.20	−3.95	−44.43
	4c	−8.15	−52.70	−0.48	−53.79	2.50	−0.89	−24.44	−2.98	−46.95
2YBF	4a	−4.15	−33.69	−1.07	−38.57	0.58	−1.75	−11.57	−0.32	−32.87
	4b	−3.03	−27.30	−1.40	−31.98	−14.55	−1.90	−8.49	−1.72	−25.29
	4c	−4.14	−34.76	−1.04	−29.97	−10.94	−1.63	−10.75	−0.84	−23.74
3HNG	4a	−7.57	−48.06	−0.48	−49.47	2.69	−1.15	−27.14	−0.65	−37.83
	4b	−9.10	−54.31	−0.93	−49.80	−13.43	-1.39	−26.76	−0.67	−48.17
	4c	−7.06	−51.24	0.00	−57.39	10.55	−2.03	−17.89	0.00	−60.47
3PJC	4a	−9.70	−43.47	−0.89	−51.15	−4.71	−1.09	−18.85	−1.07	−41.93
	4b	−6.88	−34.12	0.00	−38.33	−2.55	−0.06	−17.65	−0.10	−40.83
	4c	−8.70	−50.75	−0.48	−62.46	8.13	−0.66	−18.41	−0.88	−52.16

PARP: Poly (ADP-ribose) polymerase, VEGFR1: Vascular endothelial growth factor receptor, JAK3: Janus kinase 3

Table 2b: Molecular docking for the compounds 4a, 4b, and 4c against various key proteins such as alpha-beta tubulin, SarA, Rad6, VEGFR2, Leukocyte type core 2 beta1,6-N-acetylglucosaminyltransferase and EGFR kinase domain

PDB ID	Ligands	Molecular docking (kcaL/moL)			PDB ID	Ligands	Molecular docking (kcaL/moL)		
		Docking score	Glide energy	HBond			Docking score	Glide energy	HBond
2YB6	4a	−3.62	−32.59	−1.60	1Y6A	4a	−7.91	−46.74	−0.48
	4b	−2.59	−30.13	−1.33		4b	−7.81	−44.44	−1.63
	4c	−3.28	−32.48	−0.45		4c	−8.38	−40.91	−0.70
1TVK	4a	−5.88	−47.59	−0.55	2ITY	4a	−5.37	−41.24	−1.45
	4b	−5.90	−45.21	−1.06		4b	−6.47	−42.45	−1.18
	4c	−5.86	−43.66	−1.44		4c	−5.83	−44.55	−0.62
2FNP	4a	−5.31	−46.40	−1.27	2GAM	4a	−4.48	−41.23	−0.48
	4b	−3.73	−42.85	−0.88		4b	−5.14	−39.44	−0.95
	4c	−4.13	−48.12	−0.92		4c	−4.55	−48.58	−0.98

EGFR: Epidermal growth factor receptor, VEGFR2: Vascular endothelial growth factor receptor
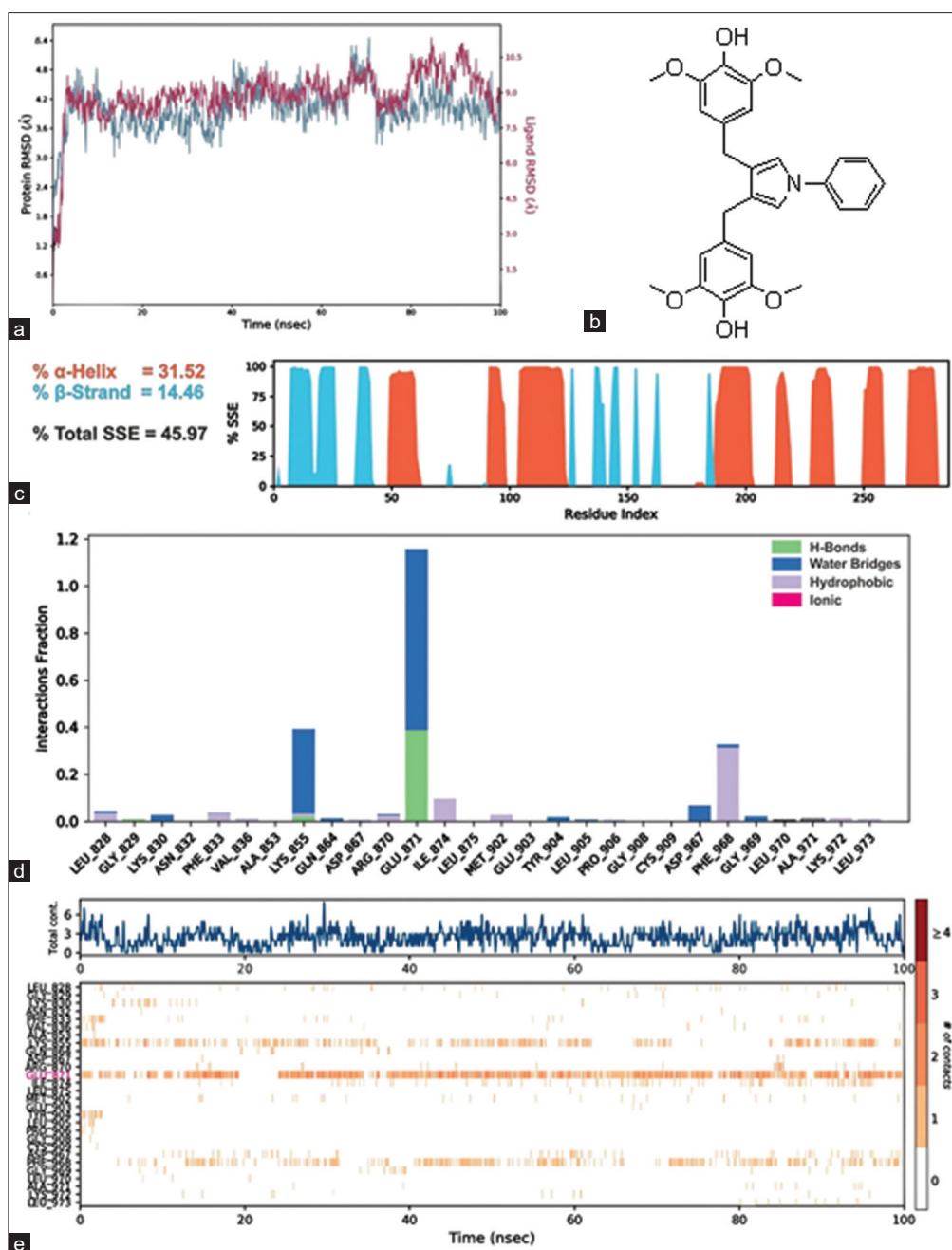
Fig. 3: Graphical representation of root-mean-square deviation (RMSD) for compound 4a with active site residues of Janus kinase 3 (JAK3) (Protein and ligand RMSD) during molecular dynamic simulation (MDS) (a). The structure of compound 4a (b). Protein secondary structure elements (SSE) distribution and its SSE assignment over time (c). Bar chart of 4a interacting with JAK3 near the putative active site pocket through a hydrogen bond, ionic bond, hydrophobic interactions and water bridges (d) and the number along with the strength of contact point of the compound 4a with JAK3 is depicted with color-coded scale bar throughout the MDS upto 100 ns (e)

MM/GBSA solvation

MM/GBSA is a method employed to determine the binding energies of protein-ligand complexes, which are important thermodynamic and desolvation factors. The favorable energies during binding are primarily due to Van der Waals and non-polar solvation effects exerted by the ligand. However, the binding process is hindered by polar solvation. The MM/GBSA scoring, which involves evaluating the binding of an individual ligand to a specific macromolecule, often correlates well with biological activity data obtained from a diverse set of ligands. The results were quantified in terms of ΔG binding energy, $\Delta G_{(Coulomb)}$, $\Delta G_{(Covalent\ energy)}$, $\Delta G_{(Hbond)}$, $\Delta G_{(Lipo)}$, and $\Delta G_{(vdW)}$ involved in the interaction (Table 1).

$$\Delta G_{(bind)} = \Delta G_{(solv)} + \Delta E_{(MM)} + \Delta G_{(SA)}$$

where:

- $\Delta G_{(solv)}$ is the difference in GBSA solvation energy of the protein-inhibitor complex and the sum of the solvation energies for unliganded protein and inhibitor.
- $\Delta E_{(MM)}$ is a difference in the minimized energies between protein inhibitor complex and the sum of the energies of the unliganded protein and inhibitor.
- $\Delta G_{(SA)}$ is a difference in the surface area energies of the complex and the sum of the surface area energies for the unliganded protein and inhibitor.
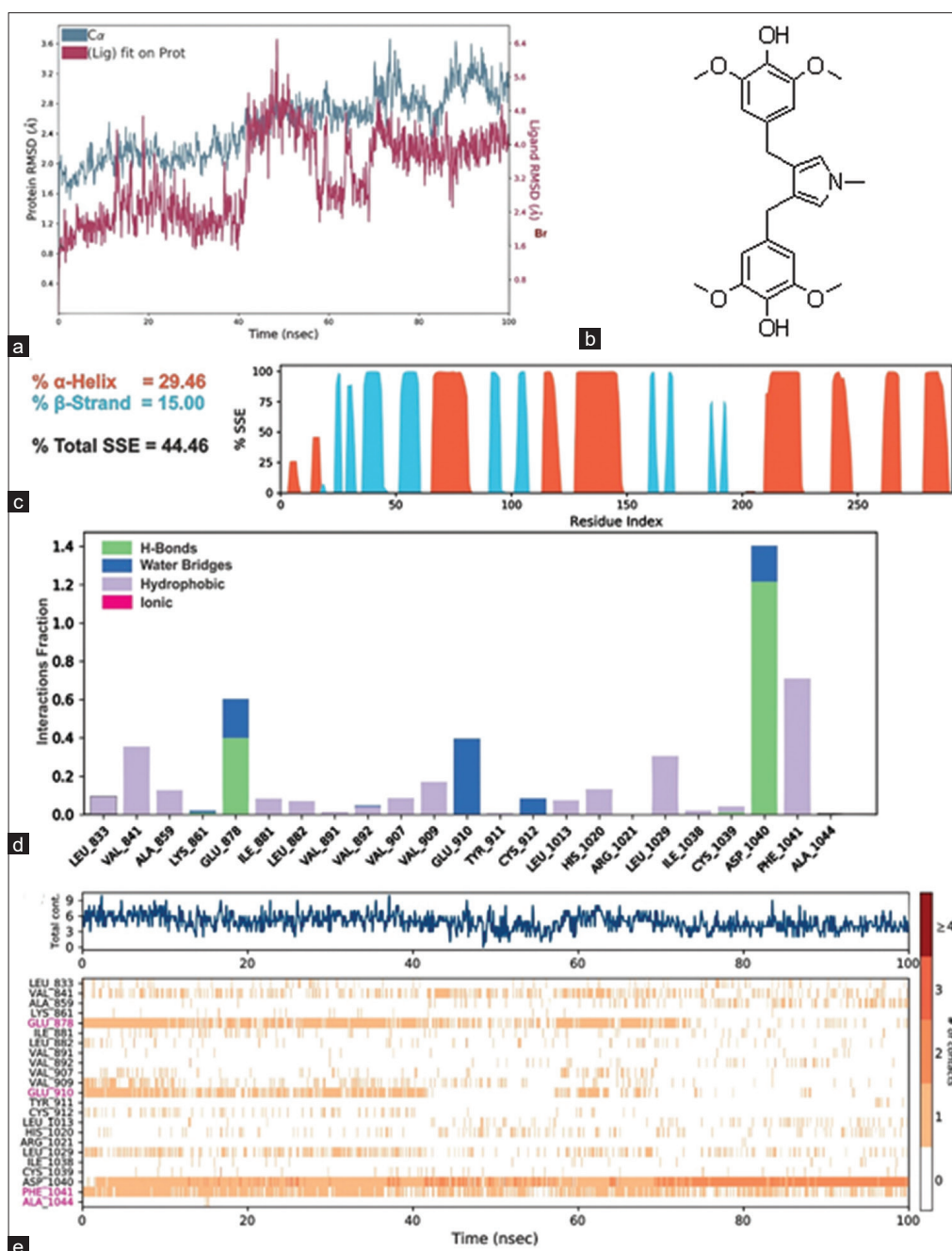
Fig. 4: Graphical representation of root-mean-square deviation (RMSD) for compound 4b with active site residues of vascular endothelial growth factor receptor (VEGFR1) (Protein and ligand RMSD) during molecular dynamic simulation (MDS) (a). The structure of compound 4b (b). Protein secondary structure elements (SSE) distribution and its SSE assignment over time (c). Bar chart of compound 4b interacting with VEGFR1 near the putative active site pocket through a hydrogen bond, ionic bond, hydrophobic interactions and water bridges (d) and the number along with the strength of contact point of the compound 4b with VEGFR1 is depicted with color-coded scale bar throughout the MDS upto 100 ns (e)

Among the calculated energies for ligands **4a, 4b,** and **4c** are the most active compounds against JAK3, VEGFR1, and PARP with higher ΔG bind values of −64.15, −49.8, and −53.79 kcaL/moL, respectively (Table 2a). Hence, ligands **4a, 4b,** and **4c** against JAK3, VEGFR1, and PARP were further subjected to MDS, to under the protein and ligand dynamics in a complex with respect to time.

MDSs

JAK3

In this study, MDS was conducted to examine the alterations in protein structure during the simulation of the protein-ligand complex

docking. The purpose of using Desmond was to stabilize the system by attaining a steady conformation, especially if the initial structure was energetically unstable. Therefore, in this particular investigation, MDS was carried out on the docked complexes of compound 4a with JAK3 (Fig. 3), and the complex was slightly stable throughout the MDS with conformational changes in the protein when the compound **4a** is bound to JAK3 (Fig. 3a). The structure of compound **4a** (Fig. 3b). It is also observed that when the MDS started at constant pressure and temperature the protein secondary structure of JAK3 undergo conformational changes in its secondary structure which is given as, alpha-helix (31.52%), and β-strands (14.46%) fluctuated very
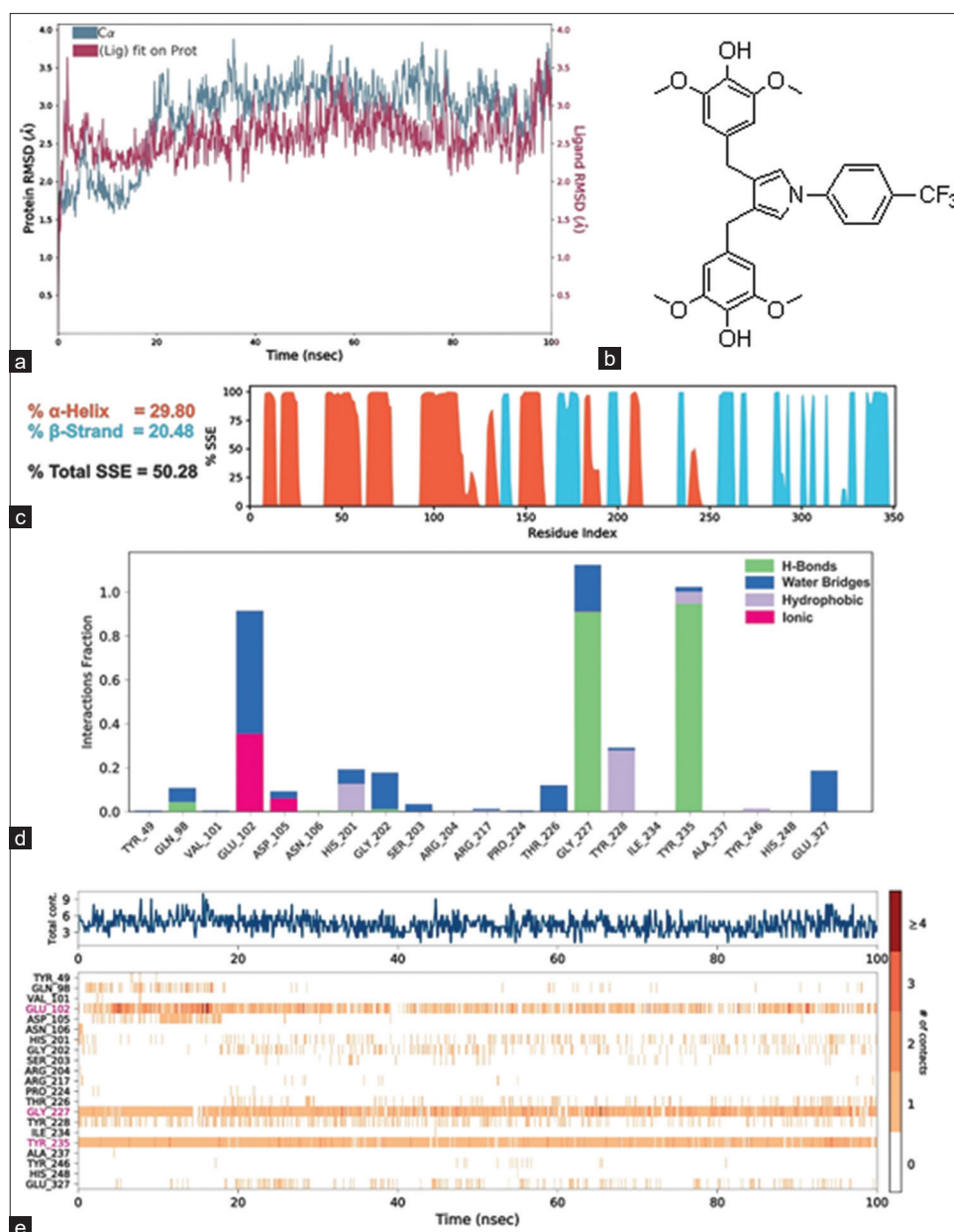
Fig. 5: Graphical representation of root-mean-square deviation (RMSD) for compound 4c with active site residues of poly (ADP-ribose) polymerase (PARP) (Protein and ligand RMSD) during molecular dynamic simulation (MDS) (a). The structure of compound 4c (b). Protein secondary structure elements (SSE) distribution and its SSE assignment over time (c). Bar chart of compound 4c interacting with PARP near the putative active site pocket through a hydrogen bond, ionic bond, hydrophobic interactions and water bridges (d) and the number along with the strength of contact point of the compound 4c with PARP is depicted with color-coded scale bar throughout the MDS upto 100 ns (e).

randomly, causing random changes in the protein resulting in the distortion of the binding site, thereby abolishing the activity of JAK3 (Fig. 3c). Normalized stacked bar chart of ligand **4a** interacting with JAK3 near the putative active site pocket through hydrophobic, hydrogen bonding along with water bridges (Fig. 3d) and the number along with the strength of contact point of the ligand **4a** with JAK3 is depicted with the color-coded scale bar wherein it is observed that Glu871very close interaction with ligand **4a** with the interaction strength of 38% (Fig. 3e).

VEGFR1

Ligand **4b** complexed with VEGFR1 was used to analysis its stability using MDSs (Fig. 4). The protein-ligand RMSD results depicted that the complex of Ligand **4b** – VEGFR1 was stable throughout the MDSs

with acceptable fluctuations from 0.8 to 2.8 Å (Fig. 4a). The structure of compound **4b** (Fig. 4b). Protein secondary structure of VEGFR1 undergo conformational changes in its secondary structure which is given as, alpha-helix (29.46%), and β-strands (15.0%) fluctuated very randomly, causing random changes in the protein resulting in the distortion of the binding site, thereby abolishing the activity of VEGFR1 (Fig. 4c). Normalized stacked bar chart of ligand **4b** interacting with VEGFR1 near the putative active site pocket through hydrophobic, hydrogen bonding along with water bridges (Fig. 4d) and the number along with the strength of contact point of the ligand **4b** with VEGFR1 is depicted with the color-coded scale bar wherein it is observed that Glu878, Glu910, Phe1041, and Ala1044 very close interaction with ligand **4b** which is observed throughout the MDSs (Fig. 4e).

PARP

Ligand **4c** complexed with PARP was used to analysis its stability using MDSs (Fig. 5). The protein-ligand RMSD results depicted that the complex of Ligand **4c**-PARP was stable throughout the MDSs (Fig. 5a). The structure of compound **4c** (Fig. 5b), ligand **4c** occupies the binding site of potent inhibitor A620223. The secondary structure of PARP when bound to ligand **4c** induced conformational changes in its alpha-helix (29.8%), and β-strands (20.48%), causing random changes in the protein resulting in the distortion of the binding site, thereby abolishing the activity of PARP (Fig. 5c). Normalized stacked bar chart of ligand **4c** interacting with PARP near the putative active site pocket through ionic, hydrophobic, hydrogen bonding along with water bridges (Fig. 5d) and the number along with the strength of contact point of the ligand **4c** with PARP is depicted with the color-coded scale bar wherein it is observed that Glu102, Gly227 and Tyr235 very close interaction with ligand **4c** which is observed throughout the MDSs (Fig. 5e).

CONCLUSION

In summary, we have attempted transition metal-free facile synthesis of LIGNAN-pyrrole derivatives in simple and short synthetic routes. We were able to attach pyrrole core into LIGNAN molecule with alkyl and aryl substitution on pyrrole ring. The cytotoxicity assay was performed for the initial evaluation of LIGNAN-pyrrole derivatives. Among the tested compounds, **4b** was emerged to be potent against HeLa cell lines at lower concentrations. Further molecular docking studies revealed that the screened compounds are found to be good PARP, VEGFR1, and JAK3 inhibitors.

AUTHOR'S CONTRIBUTION

N.C. Lohith: Data curation; Ranjini P: Methodology; Devaraju: Conceptualization and writing original draft.

CONFLICT OF INTEREST

Authors declare no conflict of interest.

FUNDING SOURCE

No external funding

REFERENCES

1. Vartak SV, Swarup HA, Gopalakrishnan V, Gopinatha VK, Ropars V, Nambiar M, *et al*. Autocyclized and oxidized forms of SCR7 induce cancer cell death by inhibiting nonhomologous DNA end joining in a Ligase IV dependent manner. FEBS J. 2018;285(21):3959-76. doi: 10.1111/febs.14661, PMID 30230716
2. Ashrafizadeh M, Aghamiri S, Tan SC, Zarrabi A, Sharifi E, Rabiee N, *et al*. Nanotechnological approaches in prostate cancer therapy: Integration of engineering and biology. Nano Today. 2022;45:101532. doi: 10.1016/j.nantod.2022.101532
3. Sharath Kumar KS, Hanumappa A, Vetrivel M, Hegde M, Girish YR, Byregowda TR, *et al*. Antiproliferative and tumor inhibitory studies of 2,3 disubstituted 4-thiazolidinone derivatives. Bioorg Med Chem Lett. 2015;25(17):3616-20. doi: 10.1016/j.bmcl.2015.06.069, PMID 26152430
4. Sharath Kumar KS, Hanumappa A, Hegde M, Narasimhamurthy KH, Raghavan SC, Rangappa KS. Synthesis and antiproliferative effect of novel 4-thiazolidinone-, pyridine- and piperazine-based conjugates on human leukemic cells. Eur J Med Chem. 2014;81:341-9. doi: 10.1016/j.ejmech.2014.05.009, PMID 24852281
5. Hegde M, Sharath Kumar KS, Thomas E, Ananda H, Raghavan SC, Rangappa KS. A novel benzimidazole derivative binds to the DNA minor groove and induces apoptosis in leukemic cells. RSC Adv. 2015;5(113):93194-208. doi: 10.1039/C5RA16605E
6. Mirzaei S, Gholami MH, Hashemi F, Zabolian A, Hushmandi K, Rahmanian V, *et al*. Employing siRNA tool and its delivery platforms in suppressing cisplatin resistance: approaching to a new era of cancer chemotherapy. Life Sci. 2021;277:119430. doi: 10.1016/j.lfs.2021.119430, PMID 33789144
7. Puneeth HR, Ananda H, Kumar KS, Rangappa KS, Sharada AC. Synthesis and antiproliferative studies of curcumin pyrazole derivatives. Med Chem Res. 2016;25(9):1842-51. doi: 10.1007/s00044-016-1628-5
8. Ananda H, Sharath Kumar KS, Nishana M, Hegde M, Srivastava M, Byregowda R, *et al*. Regioselective synthesis and biological studies of novel 1-aryl-3, 5-bis (het) aryl pyrazole derivatives as potential antiproliferative agents. Mol Cell Biochem. 2017;426(1-2):149-60. doi: 10.1007/s11010-016-2887-7, PMID 27882441
9. Lin Q, Lai R, Chirieac LR, Li C, Thomazy VA, Grammatikakis I, *et al*. Constitutive activation of JAK3/STAT3 in colon carcinoma tumors and cell lines: Inhibition of JAK3/STAT3 signaling induces apoptosis and cell cycle arrest of colon carcinoma cells. Am J Pathol. 2005;167(4):969-80. doi: 10.1016/S0002-9440(10)61187-X, PMID 16192633
10. Shibuya M. Vascular endothelial growth factor (VEGF) and its receptor (VEGFR) signaling in angiogenesis: A crucial target for anti- and pro-angiogenic therapies. Genes Cancer. 2011;2(12):1097-105. doi: 10.1177/1947601911423031, PMID 22866201
11. Chen A. PARP inhibitors: Its role in treatment of cancer. Chin J Cancer. 2011;30(7):463-71. doi: 10.5732/cjc.011.10111, PMID 21718592
12. Jagadish S, Hemshekhar M, NaveenKumar SK, Sharath KumarKS, Sundaram MS, Basappa GK, *et al*. Novel oxolane derivative DMTD mitigates high glucose-induced erythrocyte apoptosis by regulating oxidative stress. Toxicol Appl Pharmacol. 2017;334:167-79. doi: 10.1016/j.taap.2017.09.008, PMID 28911973
13. Ananda H, Sharath Kumar KS, Sudhanva MS, Rangappa S, Rangappa KS. A trisubstituted pyrazole derivative reduces DMBA-induced mammary tumor growth in rats by inhibiting estrogen receptor-α expression. Mol Cell Biochem. 2018;449(1-2):137-44. doi: 10.1007/s11010-018-3350-8, PMID 29777335
14. Ananda H, Kumar KS, Hegde M, Rangappa KS. Induction of apoptosis and downregulation of ERα in DMBA-induced mammary gland tumors in Sprague-Dawley rats by synthetic 3,5-disubstituted isoxazole derivatives. Mol Cell Biochem. 2016;420(1-2):141-50. doi: 10.1007/s11010-016-2777-z, PMID 27473146
15. Jagadish S, Rajeev N, NaveenKumar SK, Sharath Kumar KS, Paul M, Hegde M, *et al*. Platelet protective efficacy of 3,4,5 trisubstituted isoxazole analogue by inhibiting ROS-mediated apoptosis and platelet aggregation. Mol Cell Biochem. 2016;414(1-2):137-51. doi: 10.1007/s11010-016-2667-4, PMID 26899710
16. Nirgude S, Mahadeva R, Koroth J, Kumar S, Kumar KS, Gopalakrishnan V, *et al*. ST09, A novel curcumin derivative, blocks cell migration by inhibiting matrix metalloproteases in breast cancer cells and inhibits tumor progression in EAC mouse tumor models. Molecules. 2020;25(19):4499. doi: 10.3390/molecules25194499, PMID 33008036
17. Kumari S, Kotyan S, Sugunan S, Rajanikant GK, Kumar KS, Adiga SK, *et al*. The synthesis of a novel pentoxifylline derivative with superior human sperm motility enhancement properties. New J Chem. 2021;45(2):1072-81. doi: 10.1039/D0NJ03522J
18. O'Hagan D. Pyrrole, pyrrolidine, pyridine, piperidine and tropane alkaloids. Nat Prod Rep. 2000;17(5):435-46. doi: 10.1039/A707613D, PMID 11072891
19. Fan H, Peng J, Hamann MT, Hu JF. Lamellarins and related pyrrole-derived alkaloids from marine organisms. Chem Rev. 2008;108(1):264-87. doi: 10.1021/cr078199m, PMID 18095718
20. Ivan BC, Barbuceanu SF, Hotnog CM, Anghel AI, Ancuceanu RV, Mihaila MA, *et al*. New pyrrole derivatives as promising biological agents: Design, synthesis, characterization, *in silico*, and cytotoxicity evaluation. Int J Mol Sci. 2022;23(16):8854. doi: 10.3390/ijms23168854, PMID 36012121
21. Estévez V, Villacampa M, Menéndez JC. Multicomponent reactions for the synthesis of pyrroles. Chem Soc Rev. 2010;39(11):4402-21. doi: 10.1039/B917644F, PMID 20601998
22. Sharath Kumar KS, Ananda H, Rangappa S, Raghavan SC, Rangappa KS. Regioselective competitive synthesis of 3,5-bis(het) aryl pyrrole-2-carboxylates/carbonitriles vs. β-enaminones from β-thioxoketones. Tetrahedron Lett. 2021;82:153373. doi: 10.1016/j.tetlet.2021.153373
23. Lingaraju GS, Swaroop TR, Vinayaka AC, Sharath Kumar KS, Sadashiva MP, Rangappa KS. An easy access to 4,5-disubstituted thiazoles via base-induced click reaction of active methylene isocyanides with methyl dithiocarboxylates. Synthesis. 2012;44(9):1373-9. doi: 10.1055/s-0031-1290762
24. Sharath Kumar KS, Swaroop TR, Harsha KB, Narasimhamurthy KH, Rangappa KS. T3P®-DMSO mediated one pot cascade protocol for the synthesis of 4-thiazolidinones from alcohols. Tetrahedron Lett. 2012;53(42):5619-23. doi: 10.1016/j.tetlet.2012.08.020
25. Girish YR, Sharath Kumar KS, Thimmaiah KN, Rangappa KS,

Shashikanth S. ZrO2-β-cyclodextrin catalyzed synthesis of 2,4,5-trisubstituted imidazoles and 1,2-disubstituted benzimidazoles under solvent free conditions and evaluation of their antibacterial study. RSC Adv. 2015;5(92):75533-46. doi: 10.1039/C5RA13891D

26. Girish YR, Kumar KS, Manasa HS, Shashikanth S. ZnO: An ecofriendly, green nano-catalyst for the synthesis of pyrazole derivatives under aqueous media. J Chin Chem Soc. 2014;61(11):1175-9. doi: 10.1002/jccs.201400170

27. Narasimhamurthy KH, Chandrappa S, Sharath Kumar KS, Harsha KB, Ananda H, Rangappa KS. Easy access for the synthesis of 2-aryl 2,3-dihydroquinazolin-4(1H)-ones using gem-dibromomethylarenes as synthetic aldehyde equivalent. RSC Adv. 2014;4(65):34479-86. doi: 10.1039/C4RA02312A

28. Girish YR, Sharath Kumar KS, Muddegowda U, Lokanath NK, Rangappa KS, Shashikanth S. ZrO2-supported Cu(ii)-β-cyclodextrin complex: construction of 2,4,5-trisubstituted-1,2,3-triazoles via azide-chalcone oxidative cycloaddition and post-triazole alkylation. RSC Adv. 2014;4(99):55800-6. doi: 10.1039/C4RA09970B

29. Swaroop TR, Sharath Kumar KS, Palanivelu M, Chaitanya S, Rangappa KS. A catalyst-free green protocol for the synthesis of pyranopyrazoles using room temperature ionic liquid choline chloride-urea. J Heterocycl Chem. 2014;51(6):1866-70. doi: 10.1002/jhet.1864

30. Narasimhamurthy KH, Chandrappa S, Kumar KS, Swaroop TR, Rangappa KS. Synthetic utility of propylphosphonic anhydride-DMSO media: An efficient one-pot three-component synthesis of 2-Arylquinolines. Chem Lett. 2013;42(9):1073-5. doi: 10.1246/cl.130432

31. Rajeev N, Sharath Kumar KS, Bommegowda YK, Rangappa KS, Sadashiva MP. Catalyst free sequential one-pot reaction for the synthesis of 3-indole propanoates/propanoic acid/propanamides as antituberculosis agents. J Chin Chem Soc. 2021;68(1):39-44. doi: 10.1002/jccs.202000386

32. Verma SK, Verma R, Girish YR, Verma S, Pramoda K, Vaishnav Y, *et al.* Two-dimensional Ti3C2Tx MXenes as a catalyst support for the synthesis of 1,4-disubstituted-1,2,3-triazoles via azide-nitroalkene oxidative cycloaddition. J Mol Struct. 2023;1281:135145. doi: 10.1016/j.molstruc.2023.135145

33. Preetham HD, Muddegowda U, Sharath Kumar KS, Rangappa S, Rangappa KS. Identification of β-aminopyrrolidine containing peptides as β-amyloid aggregation inhibitors for Alzheimer's disease. J Pept Sci. 2022;28(6):e3386. doi: 10.1002/psc.3386, PMID 34981876

34. Verma SK, Verma R, Girish YR, Xue F, Yan L, Verma S, *et al.* Heterogeneous graphitic carbon nitrides in visible-light-initiated organic transformations. Green Chem. 2022;24(2):438-79. doi: 10.1039/D1GC03490A

35. Preetham HD, Umashankara M, Kumar KS, Rangappa S, Rangappa KS. Pyrrolidine-based cationic γ-peptide: a DNA-binding molecule works as a potent anti-gene agent. Med Chem Res. 2022;31(3):507-16. doi: 10.1007/s00044-021-02833-3

36. Zha GF, Preetham HD, Rangappa S, Sharath Kumar KS, Girish YR, Rakesh KP, *et al.* Benzimidazole analogues as efficient arsenals in war against methicillin-resistance *Staphylococcus aureus* (MRSA) and its SAR studies. Bioorg Chem 2021;115:105175. doi: 10.1016/j.bioorg.2021.105175, PMID 34298242

37. Verma SK, Verma R, Kumar KS, Banjare L, Shaik AB, Bhandare RR, *et al.* A key review on oxadiazole analogs as potential methicillin-resistant *Staphylococcus aureus* (MRSA) activity: Structure-activity relationship studies. Eur J Med Chem 2021;219:113442. doi: 10.1016/j.ejmech.2021.113442, PMID 33878562

38. Wilson Lucas S, Zijian Qin R, Rakesh KP, Sharath Kumar KS, Qin HL.

Chemical and biology of sulfur fluoride exchange (SuFEx) click chemistry for drug discovery. Bioorg Chem. 2023;130:106227. doi: 10.1016/j.bioorg.2022.106227, PMID 36368173

39. Sharath Kumar KS, Girish YR, Ashrafizadeh M, Mirzaei S, Rakesh KP, Hossein Gholami M, *et al.* AIE-featured tetraphenylethylene nanoarchitectures in biomedical application: Bioimaging, drug delivery and disease treatment. Coord Chem Rev. 2021;447:214135. doi: 10.1016/j.ccr.2021.214135

40. Verma R, Verma SK, Rakesh KP, Girish YR, Ashrafizadeh M, Sharath Kumar KS, *et al.* Pyrazole-based analogs as potential antibacterial agents against methicillin-resistance *Staphylococcus aureus* (MRSA) and its SAR elucidation. Eur J Med Chem. 2021;212:113134. doi: 10.1016/j.ejmech.2020.113134, PMID 33395624

41. Mary YS, Mary YS, Armaković S, Armaković SJ, Krátký M, Vinsova J, *et al.* Concentration and solvent dependent SERS, DFT, MD simulations and molecular docking studies of a thioxothiazolidine derivative with antimicrobial properties. J Mol Liq. 2021;329:115582. doi: 10.1016/j.molliq.2021.115582

42. Kumar AD, Vivek HK, Srinivasan B, Naveen S, Kumara K, Lokanath NK, *et al.* Design, synthesis, characterization, crystal structure, Hirshfeld surface analysis, DFT calculations, anticancer, angiogenic properties of new pyrazole carboxamide derivatives. J Mol Struct. 2021;1235:130271. doi: 10.1016/j.molstruc.2021.130271

43. Shwetha B, Sudhanva MS, Jagadeesha GS, Thimmegowda NR, Hamse VK, Sridhar BT, *et al.* Furan-2-carboxamide derivative, a novel microtubule stabilizing agent induces mitotic arrest and potentiates apoptosis in cancer cells. Bioorg Chem. 2021;108:104586. doi: 10.1016/j.bioorg.2020.104586, PMID 33607574

44. Al-Ostoot FH, Sherapura A, Vigneshwaran V, Basappa G, Vivek HK, Prabhakar BT, *et al.* Targeting HIF-1α by newly synthesized Indolephenoxyacetamide (IPA) analogs to induce anti-angiogenesis-mediated solid tumor suppression. Pharmacol Rep. 2021;73(5):1328-43. doi: 10.1007/s43440-021-00266-8, PMID 33904146

45. Shivakumar D, Williams J, Wu Y, Damm W, Shelley J, Sherman W. Prediction of absolute solvation free energies using molecular dynamics free energy perturbation and the OPLS force field. J Chem Theor Comput. 2010;6(5):1509-19. doi: 10.1021/ct900587b, PMID 26615687

46. Channa Basappa V, Hamse Kameshwar V, Kumara K, Achutha DK, Neratur Krishnappagowda L, Kariyappa AK. Design and synthesis of coumarin-triazole hybrids: Biocompatible anti-diabetic agents, *in silico* molecular docking and ADME screening. Heliyon. 2020;6(10):e05290. doi: 10.1016/j.heliyon.2020.e05290, PMID 33102875

47. Pattar SV, Adhoni SA, Kamanavalli CM, Kumbar SS. *In silico* molecular docking studies and MM/GBSA analysis of coumarin-carbonodithioate hybrid derivatives divulge the anticancer potential against breast cancer. Beni Suef Univ J Basic Appl Sci. 2020;9(1):36. doi: 10.1186/s43088-020-00059-7

48. Swamy SG, Kameshwar VH, Shubha PB, Looi CY, Shanmugam MK, Arfuso F, *et al.* Targeting multiple oncogenic pathways for the treatment of hepatocellular carcinoma. Target Oncol. 2017;12(1):1-10. doi: 10.1007/s11523-016-0452-7, PMID 27510230

49. Girish YR, Kumar BA, Kumar KS, Hamse VK, Prashantha K, Sudhanva M, *et al.* Identification of novel benzimidazole-based small molecule targeting dual targets tankyrase and Bcl2 to induce apoptosis in Colon cancer. J Mol Struct. 2022;1269:133813. doi: 10.1016/j.molstruc.2022.133813

50. Chowdary N, Preetham HD, Verma SK, Hamse VK, Umashankara M, Raj N, *et al.* A short hydrophobic peptide conjugated 3,5- disubstituted pyrazoles as antibacterial agents with DNA gyrase inhibition. J Mol Struct. 2023;1276:134661. doi: 10.1016/j.molstruc.2022.134661